NeuroImage 124 (2016) 813–823

Contents lists available at ScienceDirect

NeuroImage

journal homepage: www.elsevier.com/locate/ynimg

Characterisation and imaging of cortical impedance changes during interictal and ictal activity in the anaesthetised rat

Anna N. Vongerichten [a,*,1], Gustavo Sato dos Santos [a,1], Kirill Aristovich [a], James Avery [a], Andrew McEvoy [b], Matthew Walker [b], David S. Holder [a]

[a] Dept. of Medical Physics and Biomedical Engineering, University College London, UK
[b] Institute of Neurology, University College London, UK

ARTICLE INFO

Article history:
Received 26 May 2015
Accepted 7 September 2015
Available online 12 September 2015

Keywords:
Epilepsy
EIT
Seizure
Interictal spike
Tissue impedance
Imaging

ABSTRACT

Epilepsy affects approximately 50 million people worldwide, and 20–30% of these cases are refractory to antiepileptic drugs. Many patients with intractable epilepsy can benefit from surgical resection of the tissue generating the seizures; however, difficulty in precisely localising seizure foci has limited the number of patients undergoing surgery as well as potentially lowered its effectiveness. Here we demonstrate a novel imaging method for monitoring rapid changes in cerebral tissue impedance occurring during interictal and ictal activity, and show that it can reveal the propagation of pathological activity in the cortex. Cortical impedance was recorded simultaneously to ECoG using a 30-contact electrode mat placed on the exposed cortex of anaesthetised rats, in which interictal spikes (IISs) and seizures were induced by cortical injection of 4-aminopyridine (4-AP), picrotoxin or penicillin. We characterised the tissue impedance responses during IISs and seizures, and imaged these responses in the cortex using Electrical Impedance Tomography (EIT). We found a fast, transient drop in impedance occurring as early as 12 ms prior to the IISs, followed by a steep rise in impedance within ~120 ms of the IIS. EIT images of these impedance changes showed that they were co-localised and centred at a depth of 1 mm in the cortex, and that they closely followed the activity propagation observed in the surface ECoG signals. The fast, pre-IIS impedance drop most likely reflects synchronised depolarisation in a localised network of neurons, and the post-IIS impedance increase reflects the subsequent shrinkage of extracellular space caused by the intense activity. EIT could also be used to picture a steady rise in tissue impedance during seizure activity, which has been previously described. Thus, our results demonstrate that EIT can detect and localise different physiological changes during interictal and ictal activity and, in conjunction with ECoG, may in future improve the localisation of seizure foci in the clinical setting.

Introduction

Epilepsy is characterised by recurrent unpredictable seizures due to synchronised neuronal firing and is one of the commonest neurological conditions, affecting approximately 50 million people worldwide (Ngugi et al., 2010). Of those with chronic focal epilepsy, 20–30% will not respond to anti-epileptic drugs (Regesta and Tanganelli, 1999), yet curative epilepsy surgery remains underutilised for these patients (Wiebe and Jette, 2012). Even when such surgery is possible, over half will have seizures over the next 10 years (de Tisi et al., 2011). One major contributing factor is incorrect or incomplete focus localisation (Englot et al., 2012). There is therefore an acute clinical need for better diagnostic tools to define the location of the site of seizure onset.

Epileptic activity may be in the form of seizures which comprise intense "ictal" neuronal discharge over several seconds, or as isolated "interictal" neuronal discharges occurring between clinical seizures. Standard presurgical assessment relies upon scalp electroencephalography (EEG) and video monitoring, neuroimaging including magnetic resonance imaging (MRI), and psychometry. Several alternative methods for seizure focus localisation have been proposed, such as intrinsic optical imaging (Haglund and Hochman, 2004) and spike-triggered fMRI (Vulliemoz et al., 2010), but have not yet been widely adopted for clinical use. Potential surgical candidates often undergo intracranial EEG recordings (ECoG), where EEG electrodes are implanted directly to the surface of the cortex suspected to contain the epileptogenic focus (Rosenow and Lüders, 2001). Depth electrodes can be placed in the cortex but are limited in their spatial sampling as they damage the tissue. The present work is based on the idea that, using the same intracranial electrodes, a novel set of electrical measurements can be performed on the brain simultaneously to ECoG. These additional measurements can reveal different seizure-dependent changes in brain physiology and,

* Corresponding author at: Klinik für Neurochirurgie, Universtätsklinikum Freiburg, Breisacher Str. 64, 79106 Freiburg, Germany.
E-mail address: anna.vongerichten@uniklinik-freiburg.de (A.N. Vongerichten).
[1] Equal contributors.

http://dx.doi.org/10.1016/j.neuroimage.2015.09.015

together with ECoG, may help identify the epileptogenic area with greater accuracy.

Electrical Impedance Tomography (EIT) is an emerging medical imaging method that produces images of the internal electrical impedance of a subject from multiple surface impedance measurements (Holder, 2005). EIT has recently entered into clinical use for lung imaging in hospital ICUs (Becher et al., 2014), and has the potential for imaging brain function or pathological conditions (Boone et al., 1994; Oh et al., 2011). Localisation of the seizure onset zone has been proposed as a possible application of EIT (Boone et al., 1994); it is based on the well-established rise of impedance of cerebral tissue during seizure activity (Van Harreveld and Schade, 1962; Elazar et al., 1966). This increase in impedance can be attributed to the shrinkage of extracellular space that follows intense neuronal activity, caused by homeostatic mechanisms that redistribute water and excess potassium ions generated during the activity (Dietzel et al., 1980; Holthoff and Witte, 2000; Niermann et al., 2001). When impedance is measured at low frequencies (<50 kHz), the injected current flows mostly through the extracellular fluid and not across the highly-resistive cell membranes, and consequently any reduction in extracellular space causes a direct increase in tissue impedance (Seoane et al., 2005). Such impedance increases have been imaged with EIT using a ring of 16 electrodes placed on exposed cerebral cortex in the anaesthetised rabbit (Rao et al., 1997).

Interictal and ictal spikes may also cause a direct, transient shift in impedance. Synchronised depolarisation in a local network of neurons causes a fast drop in impedance lasting a few milliseconds due to the opening of ion channels, which allows current to flow through the highly-conductive intracellular space. These fast impedance shifts have been described in anaesthetised animals during evoked responses (Klivington and Galambos, 1967; Velluti et al., 1968; Oh et al., 2011), but never before during ictal or interictal events. EIT therefore has the unique potential to improve the localisation of epileptic foci by imaging areas of synchronised firing as well as areas of shrinkage of the extracellular space. In contrast to EEG source localisation which suffers from cancellation of dipole sources especially along sulci (Ahlfors et al., 2010), EIT has in principle a unique solution (Somersalo et al., 1992) and may be robust for localising foci throughout the brain. Furthermore, a noninvasive impedance imaging technique using MRI called MR-EIT (Kim et al., 2008) may open up a way for focus localisation without surgery.

In this study, we characterise the impedance response of cerebral tissue during interictal and ictal events in a rat model and use EIT to image these impedance changes in the cortical volume at ms temporal resolution and sub-mm spatial resolution. We induced interictal spikes (IISs) or seizures by injecting 4-aminopyridine (4-AP), picrotoxin or penicillin into the cortex of anaesthetised rats and, using highly sensitive electronic hardware, measured and imaged changes in tissue impedance during IISs and seizures. Our results show, for the first time, a rapid, transient decrease in tissue impedance preceding changes in EEG.

Materials and methods

Animal preparation

Female Sprague–Dawley rats (n = 9, 5–8 months, 300–450 g) were initially anaesthetised using isoflurane 4% in 100% oxygen, intubated (Vongerichten et al., 2014) and ventilated with 4% isoflurane in 30/70 oxygen/air. Either the femoral or the tail vein and artery was cannulated and anaesthesia was continued with: (1) 30–45 mg/kg/h α-chloralose (Sigma Aldrich Ltd., USA) for the 4-AP epilepsy group; or (2) 0.5 mg/ml droperidol (Sigma Aldrich Ltd., USA) and 10 μg/ml fentanyl, 1.5–2.5 ml/h (Martindale Pharmaceuticals Ltd., UK) for the picrotoxin and penicillin groups. Animals in the penicillin group were first relaxated with 2 mg/kg of pancuronium. Blood pressure was monitored invasively and mean arterial pressure between 90–110 mmHg was maintained using adrenaline or labetolol as necessary. Body temperature was controlled with a homeothermic heating unit (Harvard Apparatus, UK). All work was conducted under UK Home Office regulations and carried out in accordance with the Animals (Scientific Procedures) Act 1986 regulations and the European Directive 2010/63/EU on the protection of animals used for scientific purposes.

The rats were fixed in a stereotactic frame, and the skin was shaved, infiltrated with subcutaneous lidocaine and incised. The insertion of the temporal muscle on the left side was incised with a scalpel and the muscle bluntly dissected off the bone. Using a veterinary bone drill (Ideal Micro-Drill, Harvard Apparatus, UK), a craniotomy was performed reaching para-medial from 2 to 3 mm rostral to the bregma to just rostral of the lambda suture in a triangular fashion, with the tip of the triangle reaching down laterally to 1 mm above the level of the junction between zygoma and temporal bone. The bone flap was then lifted and the dura was incised. The brain was kept moist with warm (38 °C) 0.9% NaCl solution.

A 30-contact, 6 × 8 mm electrode mat was placed directly onto the cortex. It covered the hemisphere 7 mm from the rostral end to 2 mm from the caudal end in parallel to the superior sagittal sinus reaching 6 mm laterally. The electrode mat was made from stainless steel foil on a silicone rubber backing which was laser-cut to expose the 0.6-mm diameter electrodes in a hexagonal arrangement, with a centre-to-centre electrode spacing of 1.2 mm. The mat also had laser-cut holes between the contacts to allow for needle insertion. The electrodes were platinised before each experiment to reduce contact impedance. A 1 × 1 cm, silver/silver chloride reference electrode was placed under the skin on the right side of the skull, opposite the electrode mat.

Induction of epileptiform events

One of three different epileptogenic solutions was injected into the cerebral cortex: (1) 6–15 μl of 50–100 mM 4-AP (Sigma Aldrich Ltd., USA; n = 3 rats); (2) 3–10 μl of 10 mM picrotoxin (Sigma Aldrich Ltd., USA; n = 3); or (3) 6.5–20 μl of 100–200 mM penicillin (Sigma Aldrich Ltd., USA; n = 3). All solutions were prepared in 0.9% saline. Using a stereotactic micromanipulator (SM-15, Narishige, Japan), a 30G needle was advanced through a pre-cut hole in the electrode mat down a depth of 1 mm in the cortex, as measured from the brain surface. The epileptogenic solution was then injected using a syringe driver (AL1000-220, WPI, USA), and the needle was withdrawn when epileptiform changes became apparent in the ECoG. The epileptiform discharges occurred spontaneously from then on.

Simultaneous ECoG and impedance measurements

ECoG and tissue impedance were simultaneously measured by connecting the electrode mat to a multiplexed current source in parallel to a multi-channel biopotential measurement system (ActiveTwo ADbox, Biosemi, Netherlands) (Fig. 1A). The current source was a programmable, ultra-low noise constant current source with an output impedance of over 1 MΩ (details in (Oh et al., 2011)). Tissue impedance was measured by injecting a constant sinusoidal current (60 μA amplitude, 1700 Hz) between two electrodes on the mat and recording the potential on the remaining electrodes. Since the current was constant, changes in the measured voltage were proportional to changes in the underlying tissue impedance ($\Delta V = I\Delta Z$, where V is voltage, I is current and Z is impedance). Multiple sets of impedance measurements were taken by selecting different electrode pairs for the current injection. Prior to each experiment, the current source was programmed with a sequence of N electrode pairs $[(i_1,j_1), (i_2,j_2),\ldots, (i_N,j_N)]$ and injection duration T, so that initially the current was injected between electrodes i_1 and j_1 during T seconds, then between i_2 and j_2 for another T seconds, and so on until the Nth pair, after which the sequence was restarted. Electrode pairs were chosen at different distances from one another in order to have current penetrating at various depths in the tissue.

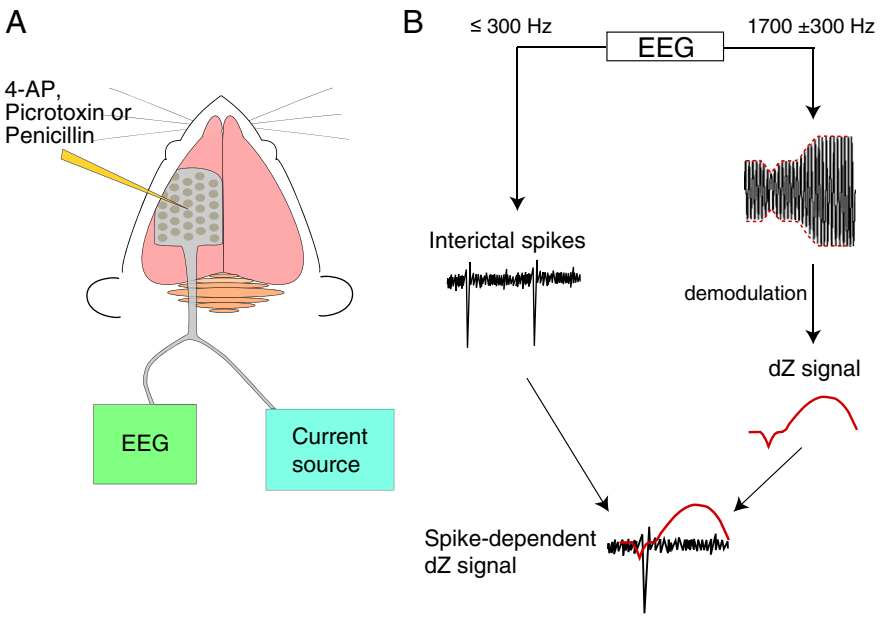

Fig. 1. Setup and signal processing for simultaneous ECoG-EIT recordings of epileptic activity. (A) A 30-electrode mat connected to an EEG amplifier and a multiplexed current source was placed on the exposed cortex of an anaesthetised rat. Impedance was measured by injecting a 60 μA, 1700 Hz sinusoidal current between a pair of electrodes on the mat. One of three epileptogenic agents – 4-AP, picrotoxin or penicillin – was injected directly in the cortex through the electrode mat. (B) The recorded broadband voltage signals were low-pass filtered at 300 Hz to recover the ECoG signals (black traces) and band-pass filtered around 1700 Hz (300 Hz bandwidth) followed by demodulation to obtain the dZ signal (red trace). The dZ signal was analysed with respect to IISs observed in the ECoG.

Furthermore, in order to maximise the number of linearly independent measurements, electrode pairs were carefully chosen so as to produce independent current patterns. That is, if electrodes are nodes in a graph and electrode pairs are edges between the corresponding nodes, then electrode pairs were selected in a way that avoided forming cycles in the graph — such as (a,b), (b,c), (a,c). This restricted the maximum number of electrode pairs to 29; the actual number used varied with the time available for the recordings. In all experiments, T was set to 15 s and N varied between 16 and 27 different electrode pairs. Having a large number of impedance measurements ensured that the cortical volume was thoroughly sampled.

Electrode potentials were measured and digitised at high sampling rate and bit depth (16 kHz sample rate, 3.2 kHz bandwidth, 24 bit ADC) and contained both ECoG and impedance signals. The ECoG and impedance signals were obtained by applying filters (fifth-order Butterworth) on the raw voltage measurements (Fig. 1B): (1) a low-pass filter with cut-off frequency at 300 Hz extracted the ECoG signals; and (2) a band-pass filter centred at 1700 Hz and with 300 Hz bandwidth (i.e., passband of 1400–2000 Hz) extracted the impedance signals. The impedance signal was subsequently demodulated by taking the amplitude of its Hilbert transform. This operation returned the amplitude envelope of the impedance signal. The phase information was not used in the present analysis, because the cortex is mostly resistive at low frequencies (Seoane et al., 2005; Logothetis et al., 2007) and the phase angle of the rat cortex in vivo was found to be less than 10° from DC to 2 kHz (Oh et al., 2011). Therefore, the reactive component was negligible and the observed impedance was almost entirely resistive.

Analysis of ECoG and impedance signals

Interictal spikes (IISs) were detected by finding negative deflections in the ECoG signals larger than 2 mV in amplitude and less than 70 ms in duration, with an interval of at least 500 ms between spikes. Only spikes that were distinct from clearly evolving electrographic seizures were included in this analysis. For each rat, the electrode recording with the largest IISs was selected as the trigger signal, and its negative peaks ("IIS triggers") were used for the analysis of impedance measurements. ECoG signals were manually annotated for seizures, which were defined as a sequence of spikes occurring at 3 Hz or higher and lasting for a minimum of 2 s. The start of the seizure was defined as the first spike in the sequence or a DC shift preceding the spikes, if present.

Impedance signals were analysed within temporal windows around the IIS triggers (from 200 ms before each trigger to 2 s after) or around the seizures (from 200 ms before the start of a seizure to 1 s after its end). Impedance change signals ("dZ signals") were obtained by normalising the impedance amplitude in each window by a baseline amplitude and subtracting 1. The baseline amplitude was defined as the average impedance amplitude during the first 150 ms in each temporal window. Because the percentage impedance changes were as low as 0.01%, impedance measurements with baseline amplitude less than 2 mV, or with baseline r.m.s. noise >5 μV were removed from analysis. Recordings from injecting electrodes were also discarded because they often saturated the DC amplifiers. Finally, in the case of IISs, impedance measurements with fewer than 10 samples (where one IIS trigger contributes one sample) were removed from analysis.

Statistical analyses were performed to determine the significance of deflections in the dZ signals. Two-tailed Student's t-test with a p-value of 0.01 was used to determine whether the average dZ value (averaged across samples) was significantly different from zero at different time points. This analysis was used for each impedance measurement to find significant negative and positive dZ signal peaks, as well as the time that the dZ signal first reached a significant positive value.

Tomographic reconstruction of impedance changes in the cortex

EIT was used to reconstruct the images of impedance changes in the cortical volume from the surface measurements. Two problems need to be solved for image reconstruction: the *forward* and the *inverse* problems. The forward problem consists of inferring the extent that changes in tissue impedance affect the measured voltages. To solve the forward problem, we assume a quasi-static approximation of Maxwell's equations so that $\nabla \cdot \sigma \nabla u = 0$ inside the volume (σ: conductivity, u: electric potential), and for the boundary conditions we use the complete

electrode model so that $\sigma\frac{du}{dv}=0$ everywhere except on the injecting electrodes where $u+z_i\sigma\frac{du}{dv}=V_i$ (v: outward unit normal, z_i: contact impedance of electrode i, V_i: voltage on electrode i) (Somersalo et al., 1992). These differential equations were solved numerically on an anatomically realistic finite element model of the rat brain obtained from an MRI, with the electrode mat placed on the cortex over the imaged volume. It comprised 7 million tetrahedral elements in the mesh (Aristovich et al., 2014a,b). The same mesh was used for every animal. The resolution of the model near the electrodes was 50 μm and gradually became coarser in depth (up to 200 μm). The brain was assumed to be isotropic and with homogeneous conductivities throughout the grey matter (at 0.3 $S\cdot m^{-1}$), white matter (0.15 $S\cdot m^{-1}$) and CSF/ventricles (1.75 $S\cdot m^{-1}$). The contact impedance of all electrodes was assumed to be 1 $k\Omega\text{-}m^2$. The finite element solver EIDORS (Adler and Lionheart, 2006) was used to compute the solution for the forward problem and to construct the Jacobian matrix J. Each entry $J_{i,j}$ in the Jacobian matrix related the extent that a conductivity change in element j in the finite element model changed the voltage measured at electrode i: $J_{i,j}=\frac{dV_i}{d\sigma_j}$.

The inverse problem refers to the estimation of the conductivity changes in the volume from the measured changes in potential. Because the changes were expected to be small, we assumed linearity so that: $\boldsymbol{\Delta V}=\mathbf{J}\Delta\boldsymbol{\sigma}$, where ΔV is the vector of measured (unnormalised) voltage changes, J is the Jacobian matrix, and $\Delta\sigma$ is the vector of conductivity changes in the volume to be estimated. The number of values to be estimated was reduced by taking an $8.4\times11\times2$ mm volume centred on the electrode mat as the region of interest, and by using a coarsened mesh with hexahedral elements for the inversion (element size: $0.2\times0.2\times0.2$ mm) (Borsic et al., 2010). However, the inverse problem was ill posed as the number of unknowns (23100) still greatly exceeded the number of measurements (~300–600). Therefore, a first-order Tikhonov regularisation was applied so that the conductivity changes were estimated as: $\Delta\hat{\boldsymbol{\sigma}}=\arg\min_{\Delta\sigma}\|\boldsymbol{\Delta V}-\mathbf{J}\Delta\boldsymbol{\sigma}\|_2^2+\boldsymbol{\lambda}\|\mathbf{L}\Delta\boldsymbol{\sigma}\|_2^2$, where λ is a regularisation parameter and L is the discrete Laplacian determined from the coarsened mesh. The optimal value for the regularisation parameter λ was determined by a cross-validation approach: for each candidate value in the search space, a cross-validated error was computed by leaving out each injection pair in the reconstruction procedure, and then using the estimated conductivity changes to predict the measurements that had been left out. The parameter value λ associated with the lowest total cross-validated error was chosen, and $\Delta\hat{\boldsymbol{\sigma}}$ was estimated using all data. The estimated conductivity changes were normalised by the assumed baseline conductivity of the grey matter (i.e., dividing by 0.3 $S\cdot m^{-1}$ and subtracting 1), converted to impedance changes ($\Delta\hat{\boldsymbol{Z}}=\frac{1}{1+\Delta\hat{\sigma}}-\mathbf{1}$) and plotted as raster images.

The number of independent measurements used for image reconstruction was larger for IIS's (300–600) than for seizures (20–30). Seizures were reconstructed from impedance data measured using single injection pairs because they often did not have a clear starting point and were highly variable in duration and intensity. In contrast, IIS's were highly repeatable and had a temporally sharp reference point (i.e., the negative peak), and therefore impedance data from multiple injection pairs were pooled for the image reconstruction. The electrographic pattern of IIS's were visually inspected, and any dissimilar samples were excluded from the data pool (<1% of samples).

Validation of image reconstruction

To validate the measurement system and the method for image reconstruction, the electrode array was placed in a 2% saline solution and impedance measurements were taken both with and without a 1-mm-diametre glass bead placed at a distance of 1 mm from the array. Similarly to the in vivo recordings, impedance measurements were obtained by injecting a constant sinusoidal current (60 μA amplitude, 1700 Hz) between two electrodes on the mat and recording the potential on the remaining electrodes. 20 different pairs of electrodes were used for the current injection (using a similar pattern as in the in vivo recordings), and a total of 600 measurements were obtained for the image reconstruction. The impedance change (dZ) was defined as the difference between the measurements with the glass bead in place and those without (the baseline). The same method for image reconstruction was used as described above, except that instead of a rat brain mesh a cylindrical mesh was used, with the electrodes placed at the bottom of the cylinder. The reconstructed image is shown in Supplementary Fig. 1; it shows a roughly spherical region of increased impedance centred at a distance of 1 mm from the electrode array.

Results

IIS-related impedance changes

Stable IISs were induced by intracortical injection of 4-AP, picrotoxin or penicillin (Fig. 1A). These chemicals trigger epileptic activity by different mechanisms – i.e., 4-AP blocks potassium channels whilst picrotoxin and penicillin block $GABA_A$ receptors – and were chosen so that the present findings are more likely to be generalisable. IISs occurred periodically at 0.2–1.5 Hz, and the amplitude of the largest IISs measured over the mat was -2.7 ± 0.4 mV in the 4-AP model (mean ± std. dev., n = 754 IISs in 2 rats), -3.5 ± 0.5 mV in the picrotoxin model (n = 2279 IISs in 3 rats), and -3.3 ± 0.7 mV in the penicillin model (n = 1699 IISs in 3 rats).

Tissue impedance was recorded simultaneously to the ECoG signals using the same electrode mat (Fig. 1). The impedance change signal ("dZ signal") exhibited a characteristic response at the time of each IIS (Fig. 2). A sharp negative deflection in the dZ signal preceded the negative peak of the IIS, and was followed by a slower rise and decay until the next IIS. This pattern in the dZ signal was observed at every IIS and in all rats tested.

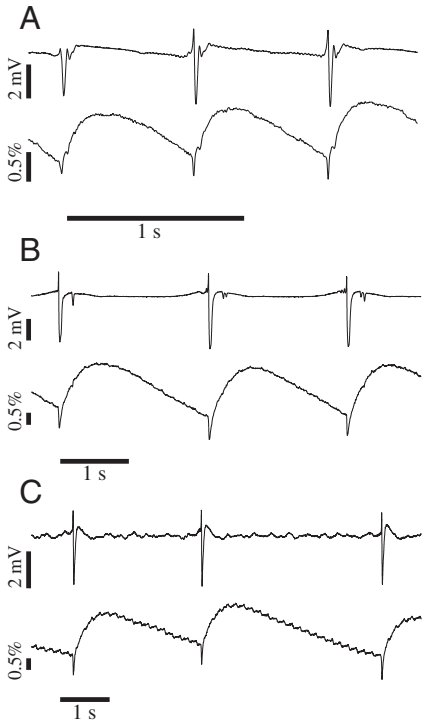

Fig. 2. Reproducible IISs and IIS-related impedance changes across three seizure models. (A) Simultaneous ECoG (top trace) and dZ signals (bottom trace) recorded from the same electrode. Stable IISs were observed in this electrode shortly after injection of 4-AP, and at each IIS the dZ signal exhibited a fast negative deflection followed by a slower rise and decay. (B–C) Same as (A), but for rats injected with picrotoxin (B) or penicillin (C).

Characteristics of the IIS-triggered dZ signals

The IISs on the channel with the largest negative deflections were used as triggers for the analysis of the dZ signals over the array. dZ signal traces were temporally aligned with respect to the negative peaks of the trigger signal and averaged over multiple IIS occurrences, given that the electrographic pattern of IIS's remained stable over the duration of the recordings. Fig. 3A presents an example set of impedance measurements displayed in the spatial arrangement of their corresponding electrodes, and ECoG signals processed with the same trigger signal are shown in Fig. 3D. IIS-triggered dZ signals had a similar waveform across electrodes but at varying amplitudes.

Multiple sets of impedance measurements were obtained by injecting the 60 μA, 1700 Hz current between different pairs of electrodes on the mat (see Methods). Changing the current injection configuration significantly altered the IIS-triggered dZ signals over the array (Fig. 3A–C), because the injected currents flowed through different regions in the volume. In contrast, the shape of the IIS did not change between configurations (Fig. 3C). By probing the cortical volume with multiple injection patterns (between 16 and 27 electrode pairs were used), we could obtain a more complete view of the impedance changes occurring in the cortex during IISs.

The amplitude and timing of the negative and positive peaks in the IIS-triggered dZ signals were analysed in each rat. Results are presented for an example rat (injected with 4-AP) in Fig. 4. In this rat, a total of 480 impedance measurements were performed using 16 different electrode pairs for the current injection. After excluding measurements from the injecting electrodes and noisy measurements (>5 μV r.m.s. noise), 371 dZ signals were kept for further analysis. Among these, significant, fast negative deflections were detected in 301 or 81% of the dZ signal traces ($p < 0.01$, Student's t-test, $n = 10$–57 IISs for each dZ signal). These negative deflections were at most −0.3% in amplitude (median: −0.04%) and preceded the IIS peak by at most −29.4 ms (median: −10 ms). Following the IIS, 324 or 87% of the dZ signal traces reached a significantly positive value within 100 ms of the IIS peak (median: 19 ms). The maximum dZ signal amplitude was 0.69% (median: 0.14%), and the maximum point was reached at a median time of 334 ms. Finally, the positive and negative peak amplitudes were significantly correlated across measurements (Fig. 4E; $r = -0.59$, $p < 0.01$, $n = 371$).

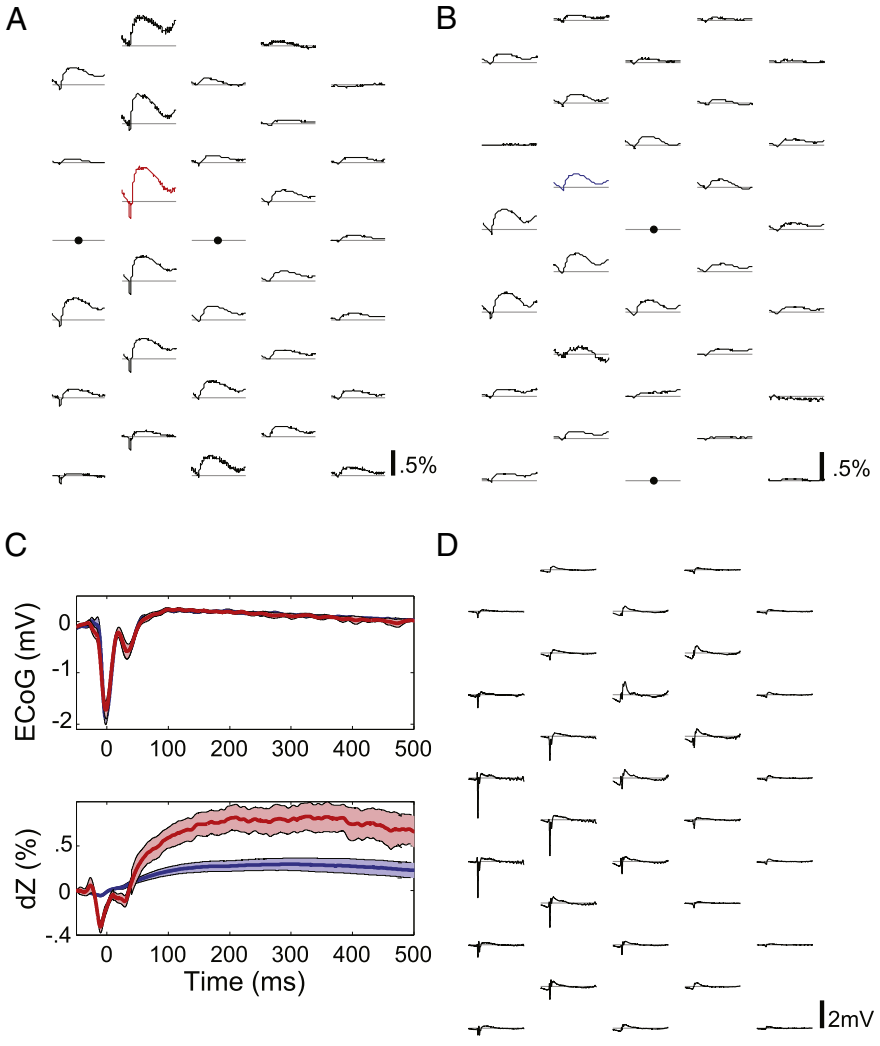

Fig. 3. Different impedance measurements were made with the same electrodes by changing the current injection configuration. (A) IIS-triggered dZ signal traces observed across the electrode mat ($n = 54$). Using the largest IIS over the array as a common trigger, the dZ signal at each electrode was aligned and averaged across IISs and are plotted at their corresponding electrode locations. Filled circles indicate electrodes used for current injection. (B) dZ signals measured using a different pair of injection electrodes ($n = 34$). (C) Comparison of ECoG (top) and dZ signals (bottom) recorded at the same electrode but using different current injection configurations. Signals measured using the configuration in (A) and (B) are shown in red and blue, respectively, and the corresponding dZ signals are indicated with the same colours in (A) and (B). Thick line: mean signal, band: 99% confidence interval for the mean ($n = 54$ or 34 IISs for the red or blue trace, respectively). (D) IIS-triggered ECoG signal pattern over the array ($n = 54$).

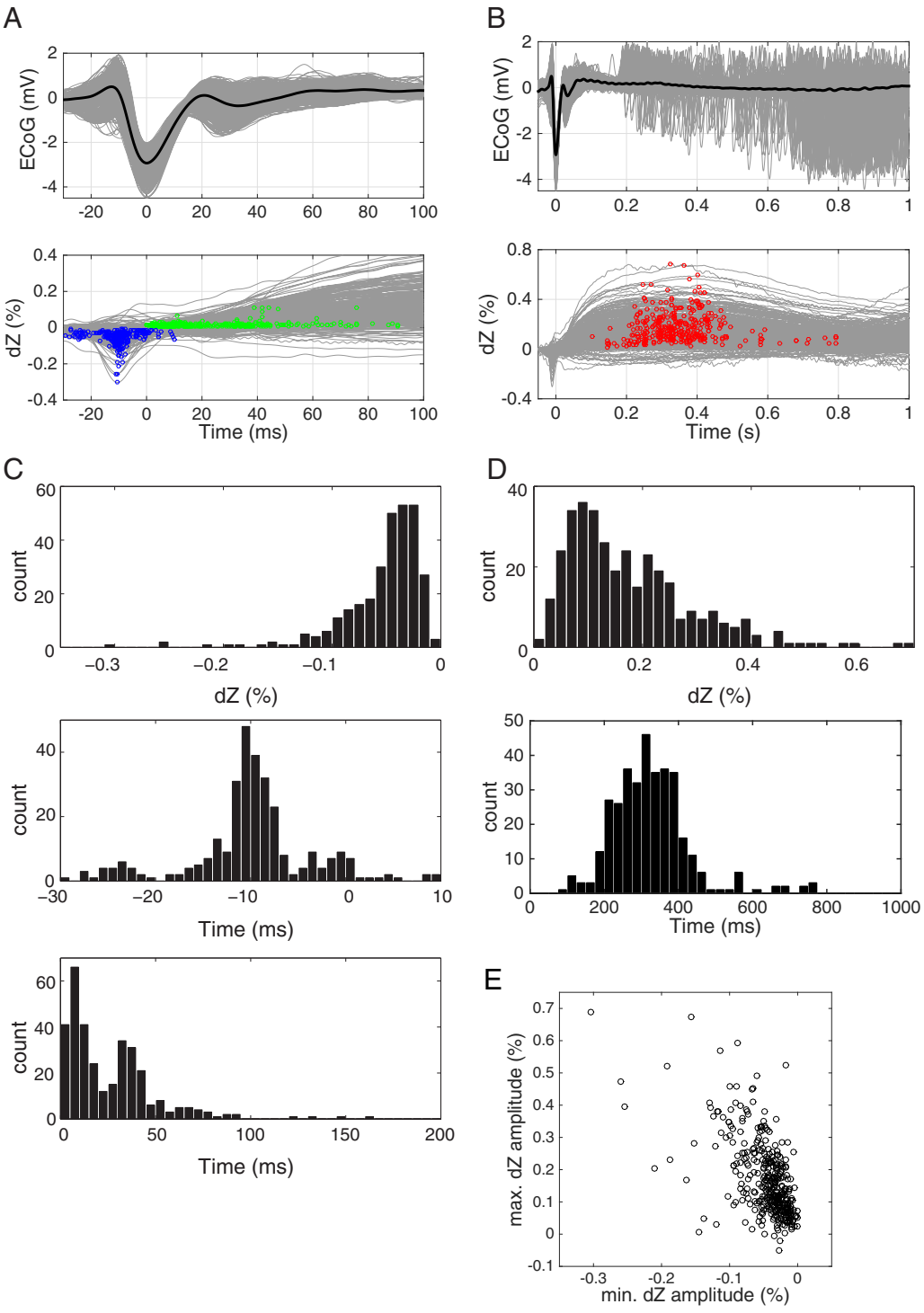

Fig. 4. Amplitude and relative timing of IIS-triggered dZ signals; data from the same recording as in Fig. 3. (A) (top) IISs at electrode with largest negative deflections (bottom left neighbour of electrode in Fig. 3), aligned by their negative peaks. Grey traces: individual IISs, thick black line: average IIS. (bottom) IIS-triggered dZ signal traces; each grey trace corresponds to the average measurement at an electrode and for a specific current injection configuration ($n = 371$ measurement combinations from 16 injection configurations). Blue circles indicate the minimum of each trace, and green circles indicate the first point reaching a significant positive value ($p < 0.01$, Student's t-test; n between 10 and 57 IISs for each trace). (B) Same data as in (A), but shown over a larger timescale. Red circles indicate the maximum of each trace. (C) Amplitude (top) and time (middle) distributions of the dZ signal minima (blue circles in (A)). (bottom) Distribution of the earliest time that dZ signals attain a positive value (green circles in (A)), expressed as onset time relative to the IIS peak. (D) Amplitude (top) and time (bottom) distributions of the dZ signal maxima (red circles in (B)). (E) Scatter plot between minimum and maximum amplitude of IIS-triggered dZ signal traces showing significant correlation ($r = -0.59$, $p < 0.01$, $n = 371$).

IIS-triggered impedance measurement produced similar results in all rats, which are summarised in Table 1. The negative peak of the dZ signal had a maximum amplitude between −0.26% and −0.93% (median values: −0.04 to −0.17%), and had a median time that preceded the IIS peak in 7 of the 8 rats tested. The only rat with positive median time nonetheless had 44% of the negative dZ signal peaks preceding the IIS peak, with the earliest one occurring at −17 ms. All rats had an increase in impedance following the IIS, with the median time to

Table 1
Summary results for the IIS-triggered dZ signals in all rats measured across all current injection configurations. The electrographic patterns of the IIS's were stable over the duration of the recordings. Fast dZ: component of dZ signal occurring around the time of the IIS peak; Slow dZ: component of dZ signal occurring after IIS; Corr: correlation between peak amplitudes of fast and slow dZ components; n IIS: number of interictal spikes used in the analysis; max. (%) and median (%): maximum and median peak amplitude in dZ signal component; t_{neg} (ms): median time of negative peak in dZ signal; t_{sig} (ms): median time when dZ signal first turns positive; t_{pos} (ms): median time of positive peak in dZ signal; and r: Pearson correlation coefficient (all $p < 0.001$).

			Fast dZ			Slow dZ				Corr.
	Rat #	n IIS	Max. (%)	Median (%)	t_{neg} (ms)	Max. (%)	Median (%)	t_{sig} (ms)	t_{pos} (ms)	r
4-AP	1	596	−0.3	−0.04	−10.0	0.69	0.14	19	334	−0.59
	2	148	−0.26	−0.07	−7.2	1.27	0.19	39	713	−0.84
Picrotoxin	1	630	−0.64	−0.12	−10.8	1.62	0.28	58	734	−0.42
	2	821	−0.42	−0.1	−6.4	0.61	0.14	32	406	−0.45
	3	828	−0.26	−0.07	−12.1	0.93	0.21	117	766	−0.87
Penicillin	1	279	−0.93	−0.13	−0.56	2.34	0.29	46	930	−0.46
	2	292	−0.47	−0.17	−1.17	1.55	0.43	62	699	−0.41
	3	1128	−0.47	−0.12	1.82	1.07	0.17	46	537	−0.52

positive dZ values ranging from 16–117 ms. Post-IIS impedance changes had a maximum amplitude of 0.61–2.34% (median values: 0.14–0.43%), with median peak times ranging between 0.34–0.93 s. Positive and negative peak dZ signal amplitudes were significantly correlated in all rats ($p < 0.01$), with correlation coefficients ranging between −0.41–0.87.

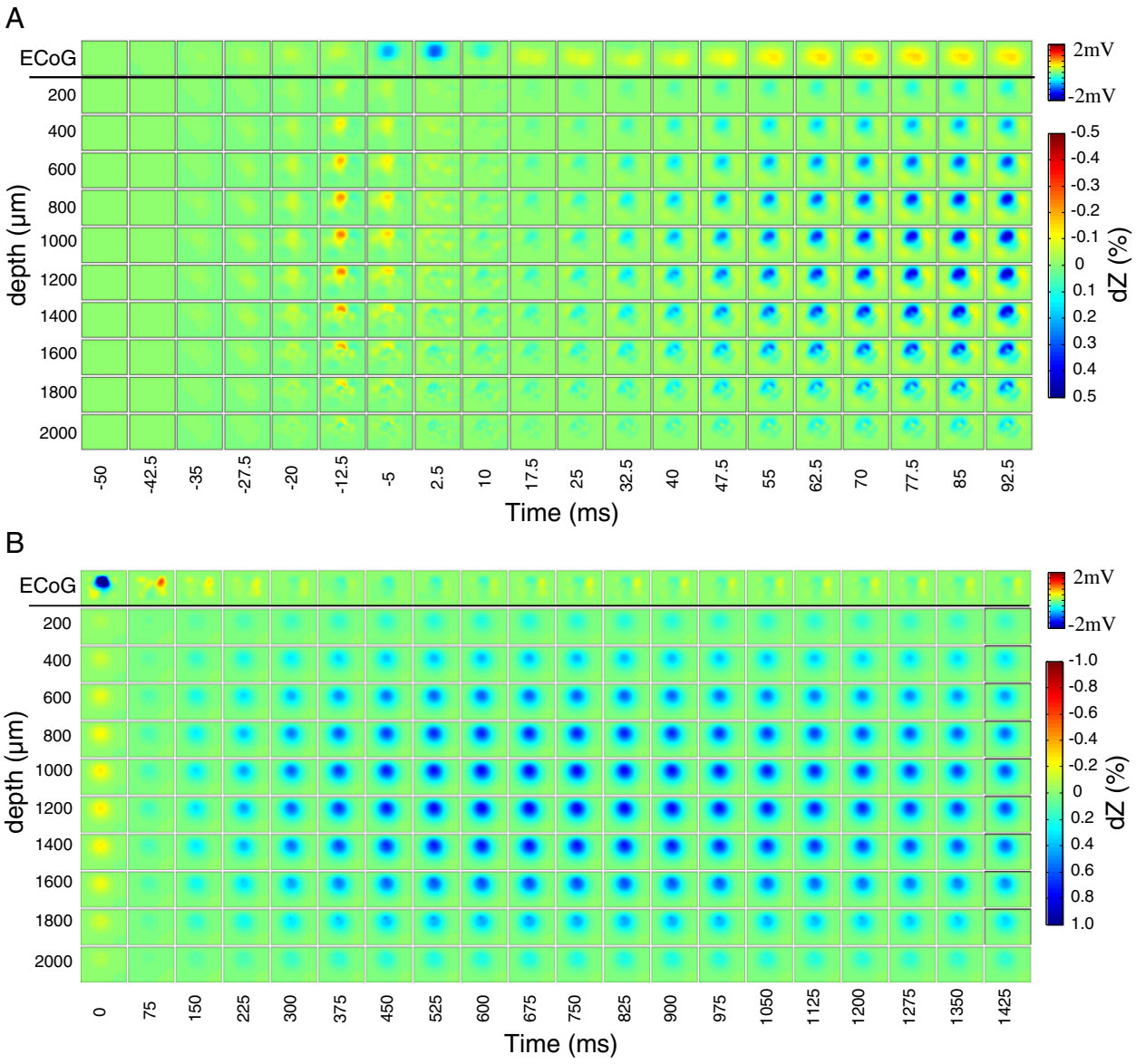

Fig. 5. Volumetric reconstruction of impedance changes from data shown in Fig. 4. Each tile is a raster image showing the estimated impedance change at a specific depth (rows; range 0.2–2 mm) and time point (columns). The first row shows the simultaneous ECoG map smoothed with a Gaussian filter (standard deviation = half the distance between adjacent electrodes). Tiles are rotated by 90° clockwise relative to the electrode maps shown in Fig. 3. (A) Impedance changes and ECoG map between −50 ms and 92.5 ms around IIS peak. Fast impedance decreases can be seen around −12.5 ms, and slow impedance increases start around 32.5–40 ms. (B) Impedance changes and ECoG map between 0 and 950 ms.

Imaging IIS-related impedance changes in the cortex

Tomographic images of cortical impedance changes were reconstructed from the IIS-triggered dZ signal datasets. Fig. 5 presents an example reconstruction using the data shown in Fig. 4. The negative dZ peak appears as a local decrease in tissue impedance of −0.4% occurring around −12.5 ms and centred at 1 mm depth (Fig. 5 top). In contrast, the IIS first becomes apparent in the ECoG map at −5 ms. These negative deflections in the ECoG and dZ images occurred over intervals of less than 25 ms. From around 40 ms, local tissue impedance increased continuously until reaching a maximum of 0.7% at 360 ms (Fig. 5 bottom). Using centre-of-mass analysis, this increase in impedance was centred at a depth of 1 mm. Tomographic impedance images were reconstructed for all rats, with similar results to the example shown. The method for image reconstruction was validated in a controlled setting (see Methods; Supplementary Fig. 1), and also in a separate experiment where EIT was used to image evoked cortical activity in anasthetised rats using depth electrodes as the gold standard (unpublished data).

The impedance changes in the reconstructed images occurred beneath the IIS region observed in the ECoG map. Raster images of the reconstructed impedance changes at 1 mm depth were compared to the ECoG map at the time of the IIS peak (Fig. 6). The negative impedance

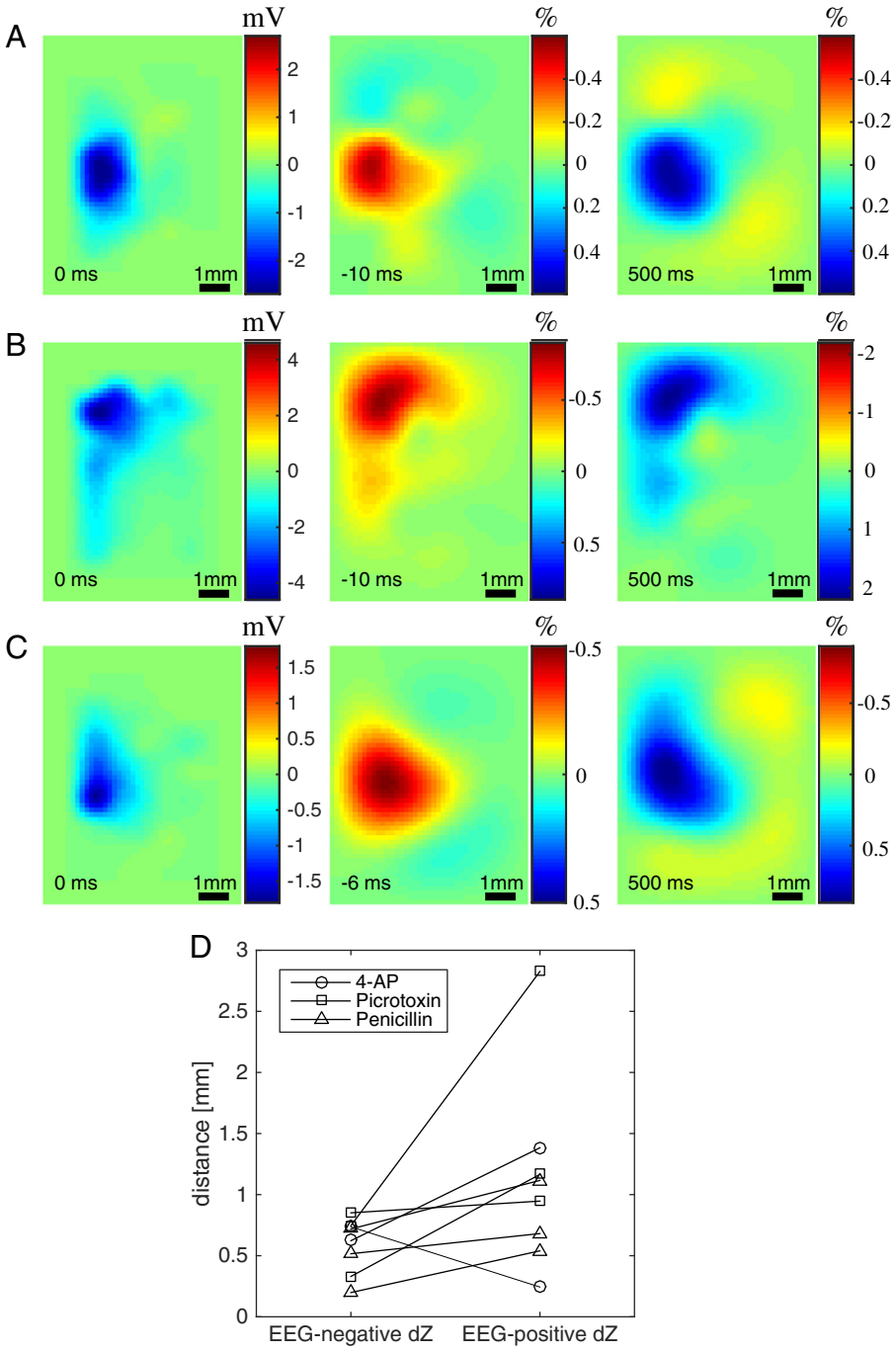

Fig. 6. Coincident location of IIS and reconstructed impedance changes. (A–C) Smoothed ECoG map (left column) and reconstructed impedance changes (middle and right columns) for three rats. The orientation of the rasters is the same as that of the electrode maps in Fig. 3. ECoG maps are shown at the time of the IIS peak, and impedance changes are shown at 1 mm depth and at the time of maximum change before the IIS peak (middle column; time shown in inset) or at 500 ms after the IIS peak (right column). Seizure models shown: 4-AP (A; same rat as in Fig. 5), picrotoxin (B) and penicillin (C). (D) Distance in mm between the centres-of-mass of the negative ECoG deflections and the impedance changes for all 8 rats.

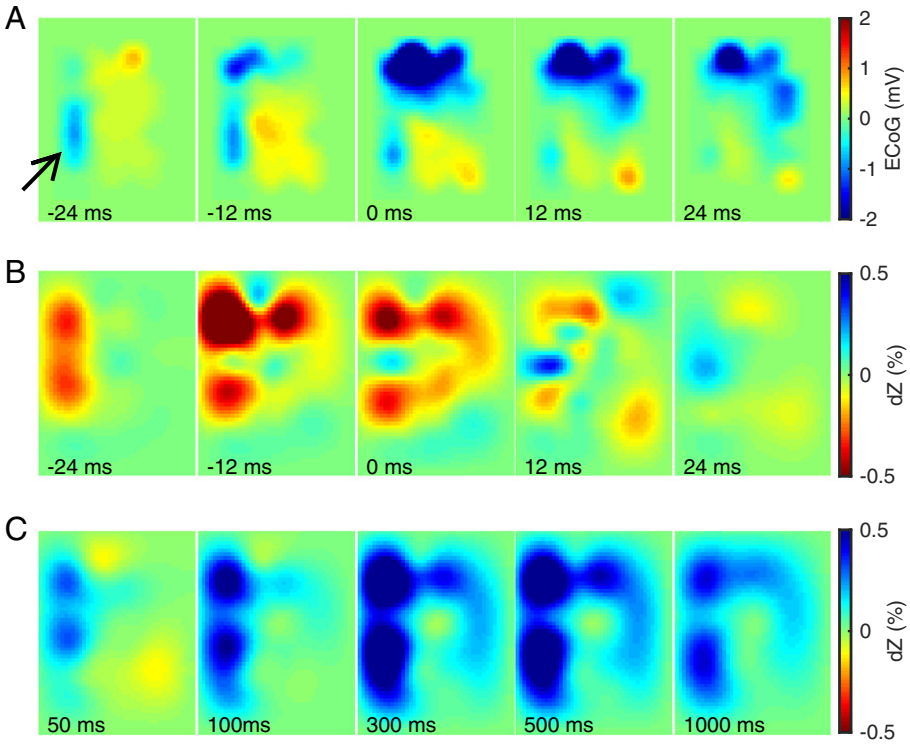

Fig. 7. Propagation of IIS in one rat (picrotoxin model). (A) ECoG map shown at 5 time points around the IIS peak (middle tile). Arrow indicates the location of negative voltage deflections preceding the main IIS. (B) Reconstructed impedance changes at 1 mm depth at the same time points as in (A). (C) Reconstructed impedance changes at 1 mm depth at 5 time points after the IIS.

changes that preceded the IIS peak were localised to the region directly below the area with the largest recorded deflections in the ECoG (Fig. 6A–C). The centre-of-mass distance in the X–Y plane between the IIS region in the ECoG map and the negative changes in the dZ map was between 0.2 and 0.85 mm (mean: 0.59 mm) across all rats and seizure models (Fig. 6D; for comparison, the diameter of the electrodes used in this experiment was 0.6 mm). However, when the same analysis was applied to the positive impedance changes observed at 500 ms, the distances to the IIS region increased to 0.24–2.83 mm (mean: 1.11 mm; Fig. 6D). The distance for one rat (picrotoxin model) stood out at 2.83 mm, as all others had been less than 1.4 mm.

To investigate why the positive impedance changes in this rat appeared to occur relatively far from the IIS region, we inspected the propagation of the activity in both ECoG and dZ maps. The ECoG map revealed that the first negative deflections had occurred at −24 ms on the lateral side of the electrode mat, but the largest spike (used as trigger in the analysis) occurred more medially and rostrally 24 ms later (Fig. 7A; Supplementary Movie M1A). This propagation was also

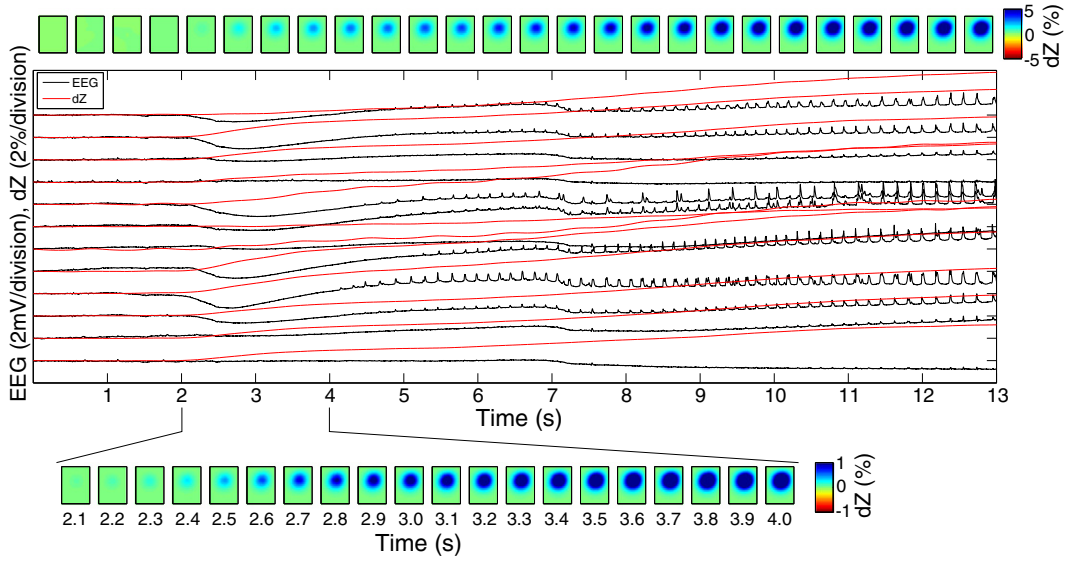

Fig. 8. Simultaneous ECoG (black) and dZ signals (red) during ictal activity in one rat (model: 4-AP). (top) Raster images showing the reconstructed impedance changes at 1 mm depth at the corresponding time points in the main graph. (bottom) Reconstructed impedance changes at 1 mm depth shown over a finer temporal scale (100 ms steps).

evident in the dZ maps, both before and after the IIS (Figs. 7B and C; Supplementary Movie M1B). The centre-of-mass distance between the negative deflections in the ECoG map at t = 0 ms and in the dZ map at t = −12 ms was only 0.74 mm, as the impedance changes had already undergone the medio-rostral shift to the region where the largest spike would be observed 12 ms later. In contrast, the dZ map at t = 500 ms still preserved a large impedance change on the lateral side of the array, which shifted the centre-of-mass away from the reference region, inflating the distance estimate to 2.83 mm. The propagation observed in this rat was more complex than in other rats, which generally exhibited a single region of activity (Supplementary Movies M2A and M2B).

Preliminary imaging of seizure activity with EIT

Measurement and reconstruction of impedance changes during seizure activity was performed in one rat that developed seizures but not IISs following the injection of 4-AP. Seizures lasting between 2 and 20 s and occurring every 8–30 s were observed in this rat (n = 74 seizure events). The beginning of seizures was characterised by a DC shift followed by an electrodecremental period of varying length, leading to spiking at 4–5 Hz frequency (Fig. 8). Impedance measurements were performed simultaneously to ECoG as in the other rats, and revealed a steady increase in impedance starting at the time of the DC shift and continuing over the duration of each seizure (Fig. 8), reaching maximum amplitudes of 2.21 ± 1.16%. Transient decreases in impedance similar to those during inter-ictal spikes were sometimes observed also during ictal spikes, but these were smaller in amplitude and swamped by the impedance increase. The EIT images revealed a region of increasing impedance centred at a depth of 1 mm, with maximum reconstructed impedance changes ranging from 0.67–13.8% (mean: 3.03%).

Discussion

The present report marks the first successful application of EIT for imaging brain impedance changes at high spatio-temporal resolution during interictal and ictal activity. Impedance changes during seizure activity have been previously reported (Van Harreveld and Schade, 1962; Elazar et al., 1966; Olsson et al., 2006; Broberg et al., 2008), but none of these studies had imaged or localised the region of changing impedance from multiple measurements. Previous efforts to image seizures with EIT in an animal model (Rao et al., 1997) showed reproducible slow changes, but had poor spatio-temporal resolution due to technical limitations. An attempt to image seizures in human patients (Fabrizi et al., 2006) suffered from excessive noise and motion artefacts due to the use of scalp electrodes. Our results demonstrate that EIT can be applied simultaneously to EEG/ECoG and produce millisecond-resolution images, which can be effectively used to track the propagation of epileptic activity (Fig. 7, Supplementary Movie M1A).

Fast cortical impedance responses preceding interictal spikes

To the authors' best knowledge, this is also the first report of fast impedance changes in cerebral tissue associated with interictal spikes. Previous impedance measurements in animal models have characterised the slow rise in cerebral tissue impedance that occurs during seizures (as in Fig. 8), but did not report rapid impedance shifts at the time of interictal or ictal spikes (Van Harreveld and Schade, 1962; Elazar et al., 1966; Olsson et al., 2006; Broberg et al., 2008). This may be attributed to the low temporal resolution used for the impedance measurements in these studies — e.g., Elazar et al. (1966) measured changes occurring between DC-2 Hz, whilst Olsson et al. (2006) and Broberg et al. (2008) low-pass filtered the impedance signal at 30 Hz. In contrast, the bandwidth of our dZ signal was 300 Hz, which provides a temporal resolution of 3.3 ms in a single measurement (averaging over multiple IISs may further increase the resolution). The duration of the fast impedance responses measured in our study was generally shorter than 15 ms — therefore, a bandwidth greater than 67 Hz would have been necessary to detect these deflections.

The fast drop in cortical impedance can be attributed to the opening of ion channels during synchronised depolarisation. A similar impedance response has been described in the cat and rat in vivo cortex during evoked activity (Klivington and Galambos, 1967; Oh et al., 2011). These studies have reported a fast drop in cortical impedance that was time-locked to evoked potentials following auditory or somatosensory stimuli. More recent measurements in the rat in vivo somatosensory cortex during forepaw stimulation, using the same hardware and signal processing as in the present work, found fast impedance changes of at most −0.26% preceding the peak of evoked potentials by 1–3 ms (Aristovich et al., 2014a,b). Validation using a depth electrode and current source-sink density analysis showed that the EIT images of the evoked responses closely matched the local field potential recorded across cortical layers, with a resolution of <200 μm (unpublished data). Altogether, these results indicate that fast impedance responses are robust indicators of synchronised cortical activity, although it is not clear which neuron types or ion channels contribute to these measurements.

Using EIT, the reconstructed fast impedance responses were centred below the IIS regions in the ECoG map (Fig. 6). Furthermore, in the 4-AP and picrotoxin models the peak of the dZ signal occurred 6–12 ms prior to the peak in the IISs (Fig. 4; Table 1). Together, these results suggest that the impedance measurements detected activity build-up prior to the IIS that had not been evident in the ECoG signals. It is well known that EEG/ECoG are mainly sensitive to synaptic activation of pyramidal neurons in superficial layers of the cortex (Mitzdorf, 1985). It may be the case, then, that our impedance measurements reflected activity synchronised by nonsynaptic mechanisms. Electrical coupling via gap junctions has been shown to play a role synchronising neurons at high frequencies and inducing seizures in animal models (Traub et al., 2001; Szente et al., 2002). More recently, it has been demonstrated in human epileptic cortex in vitro that reducing gap junction conductance reversibly abolishes very fast oscillations (VFOs) and interictal events (Roopun et al., 2010). In contrast to ECoG, impedance measurements could in principle be used to detect synchronised depolarisation of localised networks of electrically coupled neurons. If confirmed, impedance measurements can become a valuable tool for monitoring neuronal synchronisation via nonsynaptic mechanisms in pathophysiological conditions.

Impedance increase during seizures and IISs reflects shrinkage of extracellular space

The increase in tissue impedance observed after IISs (Fig. 4) and during seizures (Fig. 8) was probably due to shrinkage of extracellular space. Cell swelling and the concomitant decrease of extracellular space are well-described phenomena that have been demonstrated to follow intense activity, such as that during spreading depression (Van Harreveld and Khattab, 1967), seizures (Lux et al., 1985), and focal electrical stimulation (Dietzel et al., 1980; Holthoff and Witte, 1996, 2000). The shrinkage of extracellular space is thought to occur due to brain water and potassium homeostasis regulated by networks of glial cells. Glial cells drain water and excess potassium ions generated by intense neuronal depolarisation from middle cortical layers to superficial layers, thereby shrinking the extracellular space in the middle layers (Dietzel et al., 1980; Holthoff and Witte, 2000; Niermann et al., 2001). Our results are consistent with this phenomenon, as the reconstructed impedance increase was centred at 1 mm depth, which would correspond to layer V of the rat sensorimotor cortex (Skoglund et al., 1997). Furthermore, the reconstructed impedance increase matched the location (Figs. 5 and 6) and trajectory (Fig. 7, Supplementary Movie M1A) of the earlier, pre-IIS impedance decrease, suggesting that our method

imaged the pathological activity and subsequent extracellular space shrinkage in the same cortical region.

Post-IIS impedance changes occurred rapidly, as they were detected within 19–117 ms of the IIS and reached peak values of 0.61–2.34% within 0.3–0.9 s (Fig. 4, Table 1). In contrast, extracellular volume measured in neocortical brain slices in vitro following electrical stimulation was found to change more slowly, shrinking by a maximum of 3.5 ± 1.4% in 3.1 ± 0.3 s (Holthoff and Witte, 1996). This discrepancy may be due to physiological differences between in vitro and in vivo conditions. More recently, optical measurements in the rat neocortex in vivo have revealed metabolic changes – such as an increase in cerebral blood volume – occurring within 100 ms of the IISs (Suh et al., 2005). Faster than the increase in blood volume – which contributes negligibly to cortical tissue impedance since capillaries take up only ~2% of the cortical volume (Weiss, 1988) – was a decrease in light scattering, measured as a decrease in reflectance at 700 nm. Suh et al. (2005) found that light scattering in cortical tissue decreased by 0.09 ± 0.02% within ~1.5 s of the IIS. Since shrinkage of extracellular space has been shown to reduce light scatter (Lipton, 1973), Suh et al.'s (2005) results and our present findings may reflect the same underlying phenomenon.

Conclusion

We have characterised the impedance response of the cerebral tissue during IISs, and found that a fast, transient drop in impedance occurs before (in the 4-AP and picrotoxin models) or during (penicillin model) the interictal event, followed by a steep rise in impedance within ~120 ms of the IIS. We demonstrated that EIT can be used to reconstruct and localise these impedance changes in the cortical volume, and that the reconstructed changes were co-localised and centred at 1 mm depth, below the IIS region in the ECoG map. It is likely that the fast impedance drop reflected synchronised depolarisation in a localised network of neurons (possibly synchronised by nonsynaptic mechanisms), and that the impedance increase reflects the subsequent shrinkage of extracellular space in the same area. Finally, EIT was also used to image the steady rise in impedance during seizure activity in one rat. We thus conclude that impedance measurement and EIT are powerful tools for detecting and localising physiological changes associated with epileptic activity and, in conjunction with ECoG, may in future improve the localisation of seizure foci in the clinical setting. Towards this objective, we have developed and are testing a new EIT system with parallel current sources for measuring impedance simultaneously over multiple frequencies, capable of performing robust single-shot imaging of individual epileptiform events.

Supplementary data to this article can be found online at http://dx.doi.org/10.1016/j.neuroimage.2015.09.015.

References

Adler, A., Lionheart, W.R., 2006. Uses and abuses of EIDORS: an extensible software base for EIT. Physiol. Meas. 27 (5), S25–S42.

Ahlfors, S.P., et al., 2010. Cancellation of EEG and MEG signals generated by extended and distributed sources. Hum. Brain Mapp. 31 (1), 140–149.

Aristovich, K., et al., 2014a. High-resolution imaging of fast neural activity in the brain with electrical impedance tomography. 15th International Conference on Biomedical Applications of Electrical Impedanec Tomography.

Aristovich, K.Y., et al., 2014b. A method for reconstructing tomographic images of evoked neural activity with electrical impedance tomography using intracranial planar arrays. Physiol. Meas. 35 (6), 1095–1109.

Becher, T.H., et al., 2014. Assessment of respiratory system compliance with electrical impedance tomography using a positive end-expiratory pressure wave maneuver during pressure support ventilation: a pilot clinical study. Crit. Care 18 (6), 679.

Boone, K., et al., 1994. Imaging of cortical spreading depression by EIT: implications for localization of epileptic foci. Physiol. Meas. 15 (2A), A189–A198.

Borsic, A., et al., 2010. Electrical impedance tomography reconstruction for three-dimensional imaging of the prostate. Physiol. Meas. 31 (8), S1–S16.

Broberg, M., et al., 2008. Cell swelling precedes seizures induced by inhibition of astrocytic metabolism. Epilepsy Res. 80 (2), 132–141.

de Tisi, J., et al., 2011. The long-term outcome of adult epilepsy surgery, patterns of seizure remission, and relapse: a cohort study. Lancet 378 (9800), 1388–1395.

Dietzel, I., et al., 1980. Transient changes in the size of the extracellular space in the sensorimotor cortex of cats in relation to stimulus-induced changes in potassium concentration. Exp. Brain Res. 40 (4), 432–439.

Elazar, Z., et al., 1966. Impedance changes during epileptic seizures. Epilepsia 7 (4), 291–307.

Englot, D.J., et al., 2012. Rates and predictors of long-term seizure freedom after frontal lobe epilepsy surgery: a systematic review and meta-analysis: clinical article. J. Neurosurg. 116 (5), 1042–1048.

Fabrizi, L., et al., 2006. Factors limiting the application of electrical impedance tomography for identification of regional conductivity changes using scalp electrodes during epileptic seizures in humans. Physiol. Meas. 27 (5), S163–S174.

Haglund, M.M., Hochman, D.W., 2004. Optical imaging of epileptiform activity in human neocortex. Epilepsia 45 (s4), 43–47.

Holder, D., 2005. Electrical Impedance Tomography: Methods, History and Applications. IOP Publishing, Bristol, UK.

Holthoff, K., Witte, O.W., 1996. Intrinsic optical signals in rat neocortical slices measured with near-infrared dark-field microscopy reveal changes in extracellular space. J. Neurosci. 16 (8), 2740–2749.

Holthoff, K., Witte, O.W., 2000. Directed spatial potassium redistribution in rat neocortex. Glia 29 (3), 288–292.

Kim, H.J., et al., 2008. In vivo electrical conductivity imaging of a canine brain using a 3T MREIT system. Physiol. Meas. 29 (10), 1145.

Klivington, K.A., Galambos, R., 1967. Resistance shifts accompanying the evoked cortical response in the cat. Science 157 (3785), 211–213.

Lipton, P., 1973. Effects of membrane depolarization on light scattering by cerebral cortical slices. J. Physiol. 231 (2), 365–383.

Logothetis, N.K., et al., 2007. In vivo measurement of cortical impedance spectrum in monkeys: implications for signal propagation. Neuron 55 (5), 809–823.

Lux, H., et al., 1985. Ionic changes and alterations in the size of the extracellular space during epileptic activity. Adv. Neurol. 44, 619–639.

Mitzdorf, U., 1985. Current source-density method and application in cat cerebral cortex: investigation of evoked potentials and EEG phenomena. Physiol. Rev. 65 (1), 37–100.

Ngugi, A.K., et al., 2010. Estimation of the burden of active and life-time epilepsy: a meta-analytic approach. Epilepsia 51 (5), 883–890.

Niermann, H., et al., 2001. A novel role of vasopressin in the brain: modulation of activity-dependent water flux in the neocortex. J. Neurosci. 21 (9), 3045–3051.

Oh, T., et al., 2011. A novel method for recording neuronal depolarization with recording at 125–825 Hz: implications for imaging fast neural activity in the brain with electrical impedance tomography. Med. Biol. Eng. Comput. 49 (5), 593–604.

Olsson, T., et al., 2006. Cell swelling, seizures and spreading depression: an impedance study. Neuroscience 140 (2), 505–515.

Rao, A., et al., 1997. EIT images of electrically induced epileptic activity in anaesthetised rabbits. Med. Biol. Eng. Comput. 35 (1), 3274.

Regesta, G., Tanganelli, P., 1999. Clinical aspects and biological bases of drug-resistant epilepsies. Epilepsy Res. 34 (2), 109–122.

Roopun, A.K., et al., 2010. A nonsynaptic mechanism underlying interictal discharges in human epileptic neocortex. Proc. Natl. Acad. Sci. 107 (1), 338–343.

Rosenow, F., Lüders, H., 2001. Presurgical evaluation of epilepsy. Brain 124 (9), 1683–1700.

Seoane, F., et al., 2005. Spectroscopy study of the dynamics of the transencephalic electrical impedance in the perinatal brain during hypoxia. Physiol. Meas. 26 (5), 849–863.

Skoglund, T., et al., 1997. The existence of a layer IV in the rat motor cortex. Cereb. Cortex 7 (2), 178–180.

Somersalo, E., et al., 1992. Existence and uniqueness for electrode models for electric current computed tomography. SIAM J. Appl. Math. 52 (4), 1023–1040.

Suh, M., et al., 2005. Temporal dependence in uncoupling of blood volume and oxygenation during interictal epileptiform events in rat neocortex. J. Neurosci. 25 (1), 68–77.

Szente, M., et al., 2002. Involvement of electrical coupling in the in vivo ictal epileptiform activity induced by 4-aminopyridine in the neocortex. Neuroscience 115 (4), 1067–1078.

Traub, R.D., et al., 2001. Gap junctions between interneuron dendrites can enhance synchrony of gamma oscillations in distributed networks. J. Neurosci. 21 (23), 9478–9486.

Van Harreveld, A., Khattab, F., 1967. Changes in cortical extracellular space during spreading depression investigated with the electron microscope. J. Neurophysiol. 30 (4), 911–929.

Van Harreveld, A., Schade, J., 1962. Changes in the electrical conductivity of cerebral cortex during seizure activity. Exp. Neurol. 5 (5), 383–400.

Velluti, R., et al., 1968. Evoked resistance shifts in subcortical nuclei. Biosystems 2 (2), 78–80.

Vongerichten, A., et al., 2014. Design for a three-dimensional printed laryngoscope blade for the intubation of rats. Lab. Anim. 43 (4), 140–142.

Vulliemoz, S., et al., 2010. The combination of EEG Source Imaging and EEG-correlated functional MRI to map epileptic networks. Epilepsia 51 (4), 491–505.

Weiss, H.R., 1988. Measurement of cerebral capillary perfusion with a fluorescent label. Microvasc. Res. 36 (2), 172–180.

Wiebe, S., Jette, N., 2012. Pharmacoresistance and the role of surgery in difficult to treat epilepsy. Nat. Rev. Neurol. 8 (12), 669–677.